LCC-0062
CBP-tech Note228
May 2001

Linear Collider Collaboration Tech Notes

Symplectic Integrators for Nonlinear Wiggler Fields

Andrzej Wolski

Lawrence Berkeley National Laboratory

Abstract: To achieve fast damping, the NLC Main Damping Ring uses a wiggler with high field strength, 2.15 T, and over 45 m in length. An ideal wiggler with infinitely wide pole pieces may be treated as a linear element, and has no impact on the dynamic aperture. However, the integrated nonlinear components from a real wiggler with integrated field over 100 T^2m can be significant, and the choice of methods for studying the effects in such cases is limited at present. We present two possibilities for symplectic tracking through a wiggler taking full account of the nonlinear components of the field, compare the results with numerical integration of the equations of motion through the field in the case of the SPEAR BL11 wiggler, and consider the effects of the wiggler in the NLC Main Damping Ring.

CBP Tech Note-228
LCC-0062

Symplectic Integrators for Nonlinear Wiggler Fields

Andrzej Wolski
Lawrence Berkeley National Laboratory

April 27th, 2001

Abstract

To achieve fast damping, the NLC Main Damping Ring uses a wiggler with high field strength, 2.15 T, and over 45 m in length. An ideal wiggler with infinitely wide pole pieces may be treated as a linear element, and has no impact on the dynamic aperture. However, the integrated nonlinear components from a real wiggler with integrated field over 100 T^2m can be significant, and the choice of methods for studying the effects in such cases is limited at present. We present two possibilities for symplectic tracking through a wiggler taking full account of the nonlinear components of the field, compare the results with numerical integration of the equations of motion through the field in the case of the SPEAR BL11 wiggler, and consider the effects of the wiggler in the NLC Main Damping Ring.

1 Introduction

Wigglers are standard insertion devices in third generation light sources, and their effects on the linear dynamics are straightforward and well understood. In most cases, the nonlinear components are small, and there is little effect on the dynamic aperture of the lattice. The NLC Main Damping Rings (MDR)[1,2] need to achieve very rapid damping rates, and therefore require a long wiggler with strong field; although this would not be expected to cause problems for a short device, the fact that nearly 200 periods are needed means that the nonlinear fields must be considered carefully. A large dynamic aperture is required in the MDR for good injection efficiency. Recent experience with a new insertion device in SPEAR, the BL11 wiggler, has shown that a rapid "roll-off" of the field, resulting from narrow pole pieces, can have dramatic effect on the dynamic aperture, limiting the performance of the storage ring[3]. Although current designs for the MDR wiggler have better field quality than BL11, the wiggler will be many times longer, so the integrated effects are potentially comparable.

The dynamics in BL11 have been investigated using the code RADIA[4] to integrate numerically the equations of motion in the wiggler field. There is some correspondence between dynamical effects predicted by this model, and measurements made since the installation of the wiggler. The RADIA model was also used in the design of corrector magnets to compensate some of the nonlinear effects, and the correction is reported to be very effective. However, there are two drawbacks to the use of RADIA, that motivate the search for an alternative model:

- RADIA takes several hours to integrate through the field;
- the numerical procedure gives little information on particular features of the nonlinear components that could be affecting the dynamics.

It might be possible to simulate the effects of nonlinearities in the field by inserting thin multipoles throughout the wiggler. The main disadvantages with this technique are:

- there is no consistent and rigorous procedure for deciding the position of the multipoles, or defining their order or strength;
- the resulting field is not consistent with Maxwell's equations, and is thus non-physical.

In this note, we propose two alternative models, based on the construction of a symplectic integrator for the field, which will allow rapid calculation of the dynamic aperture, without the several hours delay resulting from numerical integration of the field. Our models also have the possible advantage that they contain information in the form of field mode coefficients that could be related to the dynamics. Since our models are based on field modes, the problem of constructing a symplectic integrator breaks down into two parts:

- the field mode coefficients must be determined from a field map;
- a symplectic map must be constructed in terms of the coefficients.

If the modes are chosen properly, then the field is guaranteed to satisfy Maxwell's equations. However, fitting a field map in three dimensions is non-trivial. Given a vector potential, the Hamiltonian for the dynamics in the wiggler may be written down straight away; however, the Hamiltonian will in general be non-integrable. Some manipulation and approximation will be required to produce a map in a closed form, suitable for implementing in a tracking code. Two different approaches to this problem will distinguish the two models we present in this note.

We begin by describing a procedure for fitting a mode expansion to a field map, and apply the procedure to the case of the SPEAR BL11 wiggler and a design for the hybrid MDR damping wiggler. We then discuss the construction of a symplectic integrator based on the mode expansion, presenting two different solutions to the problem. We apply each model to the case of the BL11 wiggler, comparing the results with those from the RADIA model. Generally, good agreement is found, particularly for the important case of the effects on the dynamic aperture. Finally, we apply our model to the NLC MDR, estimating the reduction in dynamic aperture that might be expected from the current hybrid wiggler design.

2 Fitting the Wiggler Field Map

An ideal wiggler has a (co)sinusoidal variation of the vertical field component along the beam axis. The following form for the expansion of the vertical field is then appropriate:

$$B_y = \sum_{m,n} c_{mn} \cos(k_{x,m} x) \cos(n k_z z) \cosh(k_{y,mn} y) \tag{1}$$

This is not the most general form for the field, but is sufficient for our purposes. We assume reflection symmetry in each of the three major co-ordinate planes, and this eliminates the sine terms that would otherwise appear in the series. Once we have defined the vertical field component, the horizontal and longitudinal components are determined by Maxwell's equations, which require:

$$k_{y,mn}^2 = k_{x,m}^2 + n^2 k_z^2$$

where

$$k_z = \frac{2\pi}{\lambda_w}$$

and λ_w is the wiggler period. Generally, one obtains the field map up to some limit in x; if this limit is large compared to the region of interest for beam dynamics, it is possible to arbitrarily extend the field beyond this point in any way one wishes, thus making it periodic, for example. This allows us to write:

$$k_{x,m} = mk_x$$

where k_x is fixed by the range of data. For an ideal wiggler, with infinitely wide pole-pieces, k_x tends to zero, and the field is independent of x. We can readily construct a vector potential leading to the field (1). Here, we have the additional freedom allowed by gauge invariance. For describing multipole fields, the simplest form of the Hamiltonian is given by fixing the transverse components of the potential to zero; however, in the case of the wiggler, where the field has a longitudinal dependence, only one of the components of the potential can be zero. We shall treat the transverse components as equally as possible, choosing them both to be non-zero, and fixing the longitudinal component to be zero:

$$\begin{aligned} A_x &= \sum_{m,n} c_{mn} \frac{1}{nk_z} \cos(mk_x x) \sin(nk_z z) \cosh(k_{y,mn} y) \\ A_y &= \sum_{m,n} c_{mn} \frac{mk_x}{nk_z k_{y,mn}} \sin(k_x x) \sin(nk_z z) \sinh(k_{y,mn} y) \\ A_z &= 0 \end{aligned} \tag{2}$$

and thus (for completeness, we give B_y again):

$$\begin{aligned} B_x &= -\sum_{m,n} c_{mn} \frac{mk_x}{k_{y,mn}} \sin(mk_x x) \cos(nk_z z) \sinh(k_{y,mn} y) \\ B_y &= \sum_{m,n} c_{mn} \cos(mk_x x) \cos(nk_z z) \cosh(k_{y,mn} y) \\ B_z &= -\sum_{m,n} c_{mn} \frac{nk_z}{k_{y,mn}} \cos(mk_x x) \sin(nk_z z) \sinh(k_{y,mn} y) \end{aligned} \tag{3}$$

With the form of the potential given in (2), Maxwell's equations and the symmetry conditions are satisfied. Furthermore, the periodicity of B_y in z and (by construction) in x allows us, in principle, to determine the coefficients c_{mn} by a simple two-dimensional Fourier transform of B_y in the plane $y = 0$. The fact that we have a limited range of data, and that a real field is, in general, composed of an infinite number of modes, means that the coefficients we determine from the Fourier transform, will not correspond exactly

to the field map. In practice, we find that the hyperbolic dependence of B_y on y means that small errors in the higher order coefficients, for which $k_{y,mn}$ are large, gives significant discrepancy between the fitted field and the field map, in the y direction.

Fortunately, the very sensitivity that causes the divergence in $B_y(y)$, makes the divergence easy to fix. Small corrections to the higher order coefficients can greatly improve the correspondence between the fitted field and the field map in the vertical direction, while having relatively little effect in the horizontal plane. We begin by constructing a vector $\vec{c}$, whose components c_j are just the coefficients c_{mn} listed in any order. We can then write an expression for the vertical component of the field B_y at some point $y = y_i$, $x = z = 0$:

$$B_y(y_i) = \sum_j \cosh(k_{y,j} y_i) c_j$$

Small changes to the coefficients then yield changes to the field:

$$\Delta B_y(y_i) = \sum_j \cosh(k_{y,j} y_i) \Delta c_j$$

Selecting a set of points $\{y_i\}$, we can then write:

$$\overrightarrow{\Delta B_y} = \overrightarrow{\overrightarrow{F}} \overrightarrow{\Delta c}$$

where $\overrightarrow{\overrightarrow{F}}$ is a "response" matrix with components

$$F_{ij} = \cosh(k_{y,j} y_i)$$

If we construct the vector $\overrightarrow{\Delta B_y}$ from the differences between the fitted field and the field map at selected points along the y-axis, then the changes to the coefficients required to reduce these differences to zero are just given by:

$$\overrightarrow{\Delta c} = -\overrightarrow{\overrightarrow{F^{-1}}} \overrightarrow{\Delta B_y} \qquad \textbf{(4)}$$

In general, $\overrightarrow{\overrightarrow{F}}$ is not square, or is close to singular; in which case, the inverse may be taken by singular value decomposition, and a perfect correction is not to be expected. The technique may be refined, by selecting points that vary in x as well as in y, and the changes to the above expressions are straightforward. Making changes to the coefficients of course affects the fit in the horizontal plane. However, because of the hyperbolic dependence in the vertical direction, small changes to the higher order modes that (for a well-designed wiggler) make a small contribution to the x and z dependence, effect a significant change in the y dependence.

To summarise, our procedure for fitting the mode coefficients from the field map consists of two steps:

- determine initial values for the coefficients from a Fourier transform of B_y in the plane $y = 0$;
- make (small) corrections to the coefficients to improve the fit of B_y as a function of y, using (4) above.

The variables to be considered in this procedure are:

- the range of x, which determines k_x;
- the resolution of the field map data, which determines the number of modes;
- the number and location of points y_i which are used to determine the matrix $\overrightarrow{\overrightarrow{F}}$;
- the tolerance in the singular value decomposition of $\overrightarrow{\overrightarrow{F}}$, which affects the corrections applied to the coefficients.

We have found that some trial and error is required to achieve the best fit; however, since the Fourier transform and the corrections to the Fourier coefficients can be performed with a few seconds of processor time, this is not an onerous task.

2.1 Fit to SPEAR BL11

The BL11 wiggler has 12 periods of 0.175 m, and peak field of 2 T. Narrow poles give a rapid roll-off of the vertical field beyond about 10 mm.

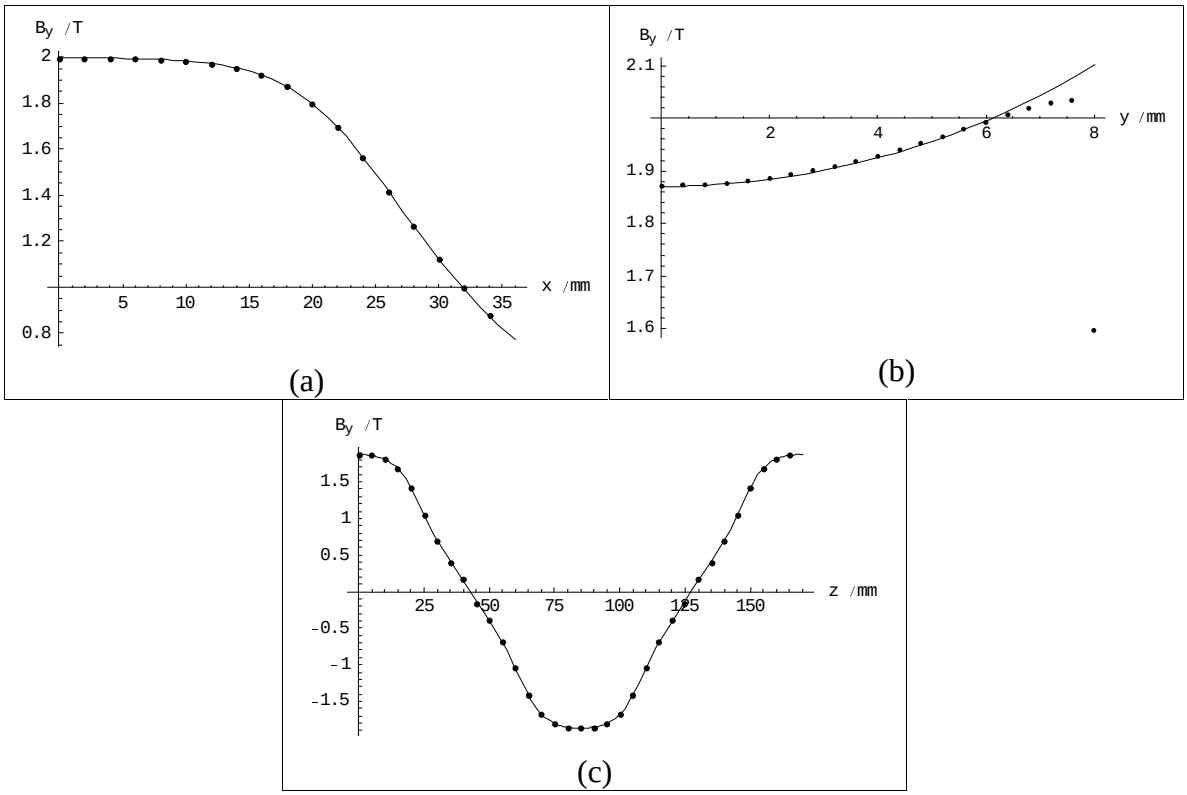

Figure 1

Vertical component of the field in SPEAR BL11 wiggler as a function of (a) x, (b) y and (c) z. Points correspond to data from the field map; lines show the fit using the Fourier transform/correction procedure.

The fit using the Fourier Transform/correction procedure using 32 modes up to 18th order is shown in Figure 1. We note that the field data suggest a rapid drop in the vertical field approaching the pole tip (the half-gap is 8 mm); we are not convinced that this is a real effect. It appears that the fit is generally good; the rms deviation in the $y = 0$ plane is 0.0027 T, and in the $z = 0$ plane is 0.0065 T. It is possible to achieve a reasonable fit using a smaller number of modes, but the deviation starts to increase rapidly, as the number of higher order modes available to effect the correction along the vertical axis reduces.

2.2 Fit to MDR Hybrid Wiggler

The data we have for this design give a peak field of 2.1 T and a period of 0.27 m. The fit using the Fourier Transform/correction procedure using 79 modes up to 34th order is shown in Figure 2. Note the scale in Figure 2(a); the drop in the vertical field at 20 mm horizontally is less than 0.3%, compared with 10% in the case of BL11.

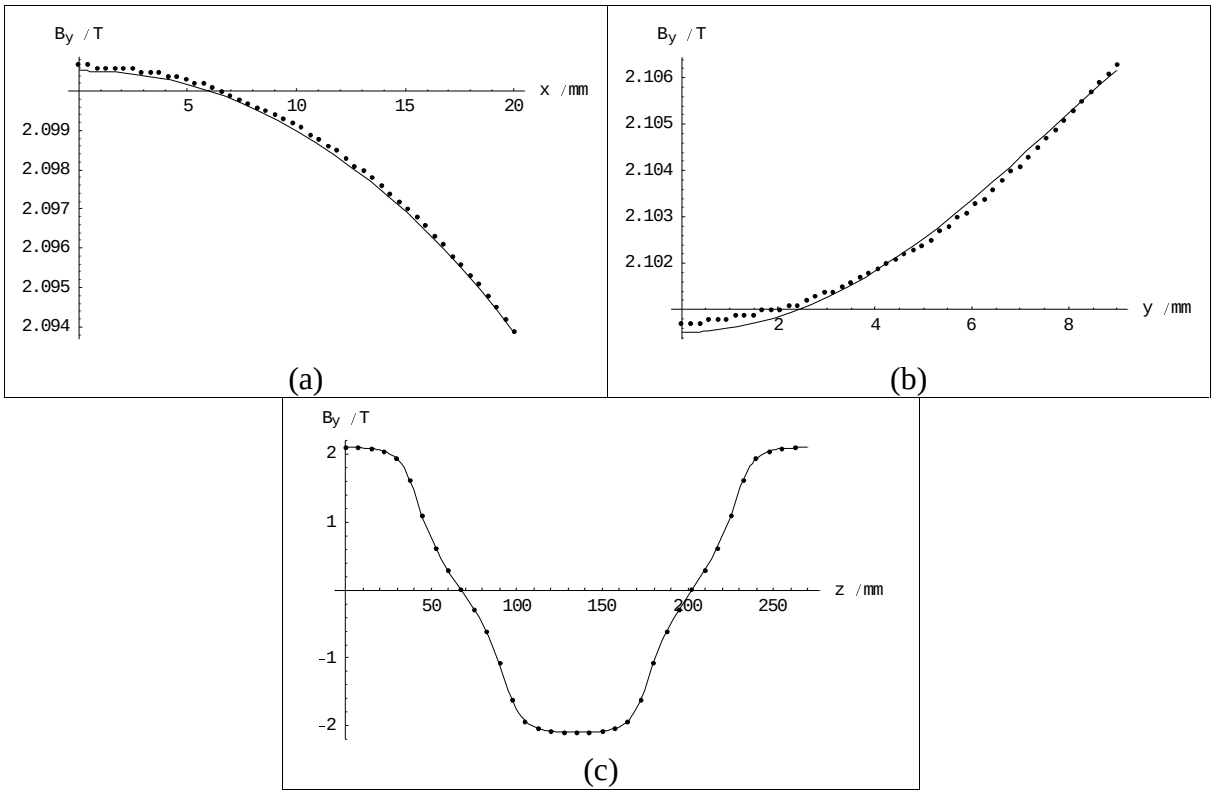

Figure 2

Vertical component of the field in MDR hybrid wiggler as a function of (a) x, (b) y and (c) z. Points correspond to data from the field map; lines show the fit using the Fourier transform/correction procedure.

The rms deviation in the $y = 0$ plane is 2.1×10^{-4} T, and in the $z = 0$ plane is 8.4×10^{-5} T. For this case, we also have data available giving B_x in the plane $z = 0$. Comparisons between the fitted field and the field map are shown in Figure 3.

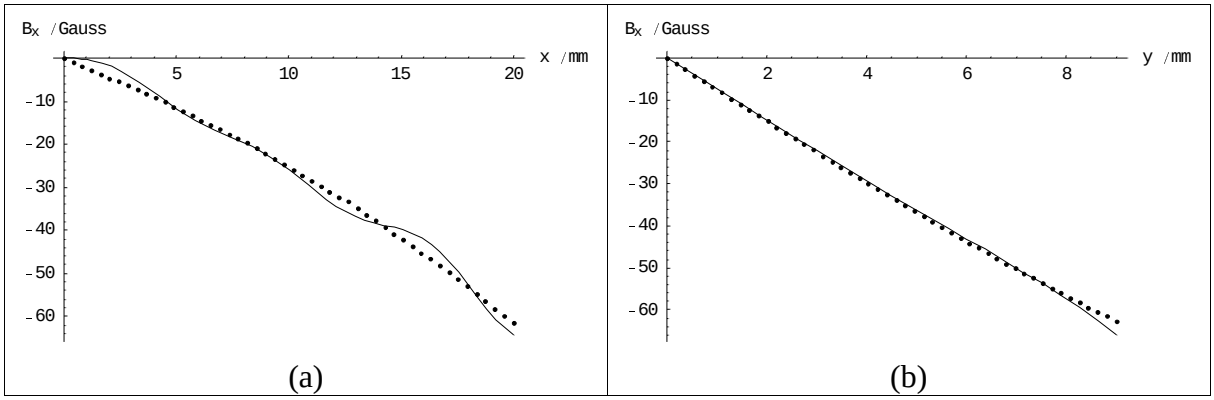

Figure 3

(a) B_x as a function of x at $y = 9$ mm and $z = 0$, and (b) B_x as a function of y at $x = 20$ mm and $z = 0$. Note the vertical axes in gauss.

We note that the data for B_x were not used in the fitting procedure at all. The close correspondence between the fitted field and the field map shown in Figure 3 are therefore encouraging, particularly as the data are near the limit of the expected range of validity ($y = 9$ mm or $x = 20$ mm).

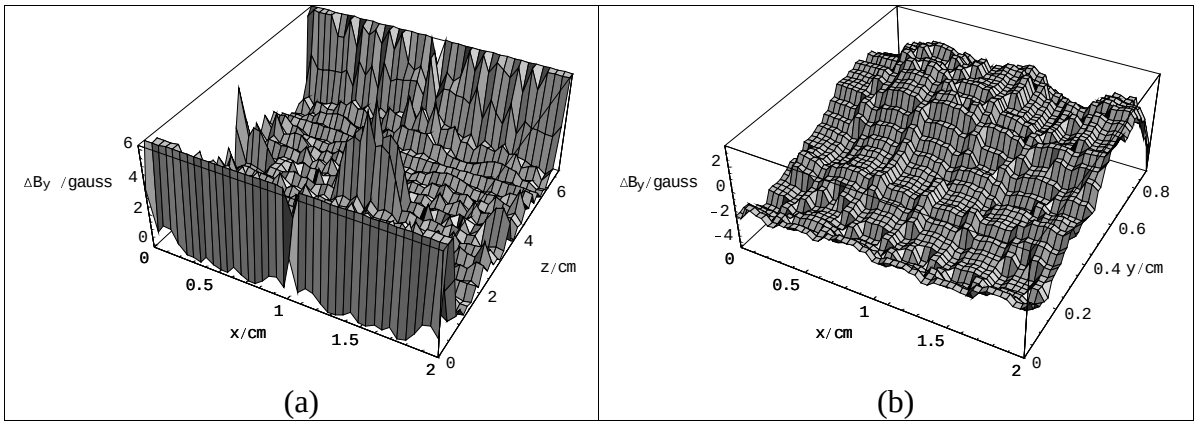

Figure 4

Vertical field deviation between the fitted field and the field map (a) in the $y = 0$ plane, and (b) in the $z = 0$ plane. Note the vertical scale in gauss in each plot.

The fit to the field map is good, but at the cost of a large number of field modes. As in the case of SPEAR BL11, reducing the number of field modes leads to a rapid increase in the deviation between the fitted field and the field map. However, we feel that we have, in principle, a technique for determining the mode coefficients such that the field map may be fitted with very good accuracy. In the case of the MDR hybrid wiggler, the deviation of the vertical field component in the planes $y = 0$ and $z = 0$ is lower than 0.03% of the wiggler peak field.

3 Symplectic Integrator

3.1 Full Symplectic Integrator

Having obtained an expansion of the field, we can proceed to derive a map describing the particle dynamics in the wiggler. We begin with the standard Hamiltonian with longitudinal displacement s as the independent variable:

$$H = -\sqrt{(1+\delta)^2 - (p_x - a_x)^2 - (p_y - a_y)^2} - a_z$$

where the transverse momenta are normalized with respect to the longitudinal momentum p_0, and

$$\vec{a} = \frac{e\vec{A}}{p_0} = \frac{\vec{A}}{B\rho}$$

We have chosen a gauge such that $a_z = 0$. Using this, and expanding the Hamiltonian for $(p_i - a_i)^2 << 1$, we find the approximation:

$$H \approx -(1+\delta) + \frac{p_x^2 + p_y^2}{2(1+\delta)} + \frac{a_x^2 + a_y^2}{2(1+\delta)} - \frac{a_x p_x + a_y p_y}{(1+\delta)} \tag{5}$$

The first two terms in (5) generate a drift, and the third term gives a transverse momentum "kick". The fourth term, involving a coupling between the momenta and the co-ordinates, is non-integrable: we assume this term can be dropped if we average the Hamiltonian over one period of the wiggler. In a further approximation, we factorise the map with the kick term between two half-length drifts.

Using the expressions for the potential given in (2), we find:

$$\begin{aligned}
\left\langle a_x^2 \right\rangle &= \frac{1}{2(B\rho)^2 k_z^2} \sum_{\substack{m,m' \\ n\neq 0}} \frac{c_{mn} c_{m'n}}{n^2} \cos(mk_x x)\cos(m'k_x x)\cosh(k_{y,mn} y)\cosh(k_{y,m'n} y) \\
\left\langle a_y^2 \right\rangle &= \frac{k_x^2}{2(B\rho)^2 k_z^2} \sum_{\substack{m,m' \\ n\neq 0}} \frac{mm' c_{mn} c_{m'n}}{n^2 k_{y,mn} k_{y,m'n}} \sin(mk_x x)\sin(m'k_x x)\sinh(k_{y,mn} y)\sinh(k_{y,m'n} y)
\end{aligned} \tag{6a}$$

and we use the Hamiltonian:

$$H_{\text{kick}} = \frac{\left\langle a_x^2 \right\rangle + \left\langle a_y^2 \right\rangle}{2(1+\delta)} \tag{6b}$$

From now on, we drop the "kick" subscript, and simply denote the kick Hamiltonian by H. Note that we have dropped terms corresponding to the zeroth-order longitudinal mode, $n = 0$. These may be included in our treatment, but simply contribute additional terms, that vanish if the integrated field along the axis is zero. This condition is usually satisfied in wigglers.

The actual momenta kicks are readily derived from:

$$\Delta p_x = -\lambda_w \frac{\partial H}{\partial x}$$
$$\Delta p_y = -\lambda_w \frac{\partial H}{\partial y} \qquad (6c)$$

where λ_w is the wiggler period. The resulting expressions are straightforward if somewhat lengthy; we feel there is no need to give them explicitly here. They may be readily incorporated into a tracking code. Equations (6a), (6b) and (6c) constitute our full symplectic integrator model.

It is interesting to consider the special case of a "semi-ideal" wiggler, that is one which has infinitely wide pole pieces, so no dependence of the field on x, but the field variation along the axis may not be exactly sinusoidal. For such a device, as we remarked above, we take the limit $k_x \to 0$. Expressions (6a) then reduce to the simple form:

$$\left\langle a_x^2 \right\rangle = \frac{1}{2(B\rho)^2 k_z^2} \sum_{n\neq 0} \frac{c_n^2}{n^2} \cosh^2(nk_z y)$$
$$\left\langle a_y^2 \right\rangle = 0$$

Expanding the hyperbolic cosine as a series, we obtain (for $\delta = 0$):

$$H = \frac{\left\langle a_x^2 \right\rangle}{2} = \frac{1}{4(B\rho)^2 k_z^2} \sum_{n'} \left(\sum_{n\neq 0} c_n^2 n^{2n'-2} \right) b_{2n'} (k_z y)^{2n'} \qquad (7)$$

where

$$b_{2n'} = \sum_{l=0}^{n'} \frac{1}{(2l)!(2n'-2l)!}$$

The $n' = 0$ term in (7) is independent of the co-ordinates, so makes no contribution to the dynamics. The $n' = 1$ term is a vertical focusing, with strength:

$$K_1 = \frac{1}{2(B\rho)^2} \sum_n c_n^2 = \frac{1}{\lambda_w (B\rho)^2} \int_0^{\lambda_w} B^2 \mathrm{d}s \qquad (8)$$

Hence the linear focusing for a wiggler with infinitely wide pole-pieces agrees with that for the hard-edged dipole model of the wiggler, and this is independent of the form of the variation of the vertical field along the axis.

Terms in (7) with $n' \geq 2$ give tune shifts with amplitude of increasingly high order. For a cosinusoidal variation of the field, we have:

$$\left\langle a_x^2 \right\rangle = \frac{\hat{B}_w}{2(B\rho)^2 k_z^2} \sum_{n'} b_{2n'} (k_z y)^{2n'}$$

where $\hat{B}_w$ is the peak wiggler field; the higher order tune shifts may be readily worked out. An interesting situation occurs when we try to apply equation (7) to the hard-edged

dipole model, where the field varies as a square wave along the axis. Then we have that $c_n \sim 1/n$, and it appears that we have a divergent factor in all the nonlinear terms. However, this is a linear model, and all the nonlinear terms should vanish. It is not clear to us at present how to resolve this situation; we suspect that the apparent inconsistency arises from the attempt to apply a model that is consistent with Maxwell's equations to a hard-edged field model that is strictly not physical.

3.2 Reduced Harmonic Model

As we noted above, expressions (6a), (6b) and (6c) together form a model for the dynamics in the wiggler that takes account of the nonlinear fields in a physical way. We have made approximations in averaging over the wiggler period, and separating the Hamiltonian into integrable factors. However, our final map is symplectic and consistent with Maxwell's equations: it does not break any physical laws, though it may not correspond exactly to the observed dynamics. The disadvantage with the full symplectic integrator, is that it is necessary to evaluate a triple summation. For a fit to the field map in the MDR wiggler, we used 79 field modes; in such a case, the processor time required for each step through the wiggler, corresponding to a singe period, becomes significant (although generally still somewhat faster than a detailed numerical integration through the field map). It is possible, of course to speed the tracking by reducing the number of field modes used. However, one then sacrifices some of the accuracy of the representation of the wiggler field, and even for a smaller number of modes, the triple summation still slows the tracking considerably.

Calculation of the dynamic aperture in the NLC main damping rings, where there are nearly 200 wiggler periods, will typically require several tens of thousands of particle turns. This motivates our search for a more efficient symplectic integrator that will avoid the triple summation involved in the full symplectic integrator. A possible approach is to assume that a particle follows a sinusoidal trajectory through a single period of the wiggler. For a wiggler with a field varying sinusoidally along the axis, this is a good approximation. Using this model, it is easy to understand the effect of a roll-off of the vertical field in the x direction. A particle entering the wiggler off-axis, will see a greater vertical field at one side of the trajectory than the other, resulting in a net transverse kick. The size of the kick clearly depends on the size and gradient of the field; thus, we expect the kick to increase with horizontal displacement from the axis, peak where the roll-off becomes steep, then fall as the field strength itself falls off.

To consider this in a little more detail, let us look at the case where the wiggler field is given by:

$$B_y = \hat{B}_w \cos(k_z z)\cos(k_x x)\cos(k_y y)$$

where $k_y^2 = k_x^2 + k_z^2$. Restricting the motion to the plane $y = 0$, we can write the following expression for the integrated field seen by the particle in one wiggler period:

$$\begin{aligned} \int B_y \mathrm{d}s &= \int_0^{2\pi/k_z} \cos(k_z z)\cos\left(x_0 + a\cos(k_z z)\right)\mathrm{d}z \\ &= -\lambda_w \sin(x_0)\mathrm{J}_1(a) \end{aligned} \tag{9}$$

where x_0 is the initial horizontal co-ordinate of the particle, and

$$a = \frac{\hat{B}_w \cos(k_x x_0)}{(B\rho)^2 k_z^2}$$

is the amplitude of the particle's oscillation as it passes through the wiggler period. $\mathrm{J}_n(a)$ is a Bessel function of the first kind. The integrated field from (9) gives the horizontal momentum kick. However, we need to take account of the full set of field modes, and the associated vertical kick that will be present if the motion is off the mid-plane. Symplecticity is assured if we derive the kicks from a generating function (Hamiltonian), using (6c). We require the Hamiltonian to give the correct vertical focusing (8), the correct horizontal kick (9), and to be a good approximation to the full symplectic integrator given in (6). We propose the following form for the kick Hamiltonian:

$$H = \frac{1}{2B\rho} \sum_{mn} c_{mn} \cos(mk_x x) \mathrm{J}_n(f) \cosh(k_{y,mn} y) \tag{10a}$$

where

$$f = \frac{B_y(x, y, z=0)}{(B\rho) k_z^2} \tag{10b}$$

We do not claim to have a rigorous justification for the expression (10a). However, it is clear that, for infinitely wide pole pieces, and with a single longitudinal mode:

$$\underset{k_x \to 0}{\mathcal{L}t}\ H = \frac{\hat{B}_w^2 \cosh^2(k_z y)}{4(B\rho)^2 k_z^2}$$

so we have the correct linear vertical focusing. The reduced harmonic form given in (10) has the advantage over the full symplectic integrator, that it reduces the number of terms in the summation, and is significantly faster to evaluate; in fact the number of terms in the summation increases only linearly with the number of modes in the field expansion, rather than (roughly) as the square.

The momenta kicks are again given by (6c); the expressions are easy to derive, and we do not give them explicitly.

4 Application to SPEAR BL11

The field expansion using 32 modes has already been obtained in Section 3.1; the full symplectic integrator and reduced harmonic model can be applied directly. In addition, the dynamical map produced using RADIA is available for BL11, allowing a direct comparison of three different models. We note that RADIA integrates the equation of motion through the wiggler, producing a table of horizontal and vertical kicks. We have implemented the full symplectic integrator and reduced harmonic model in the tracking code MERLIN[5]; the corresponding kick tables are produced in a few seconds rather than the several hours taken for numerical integration.

The horizontal and vertical kicks as functions of x are shown in Figure 5.

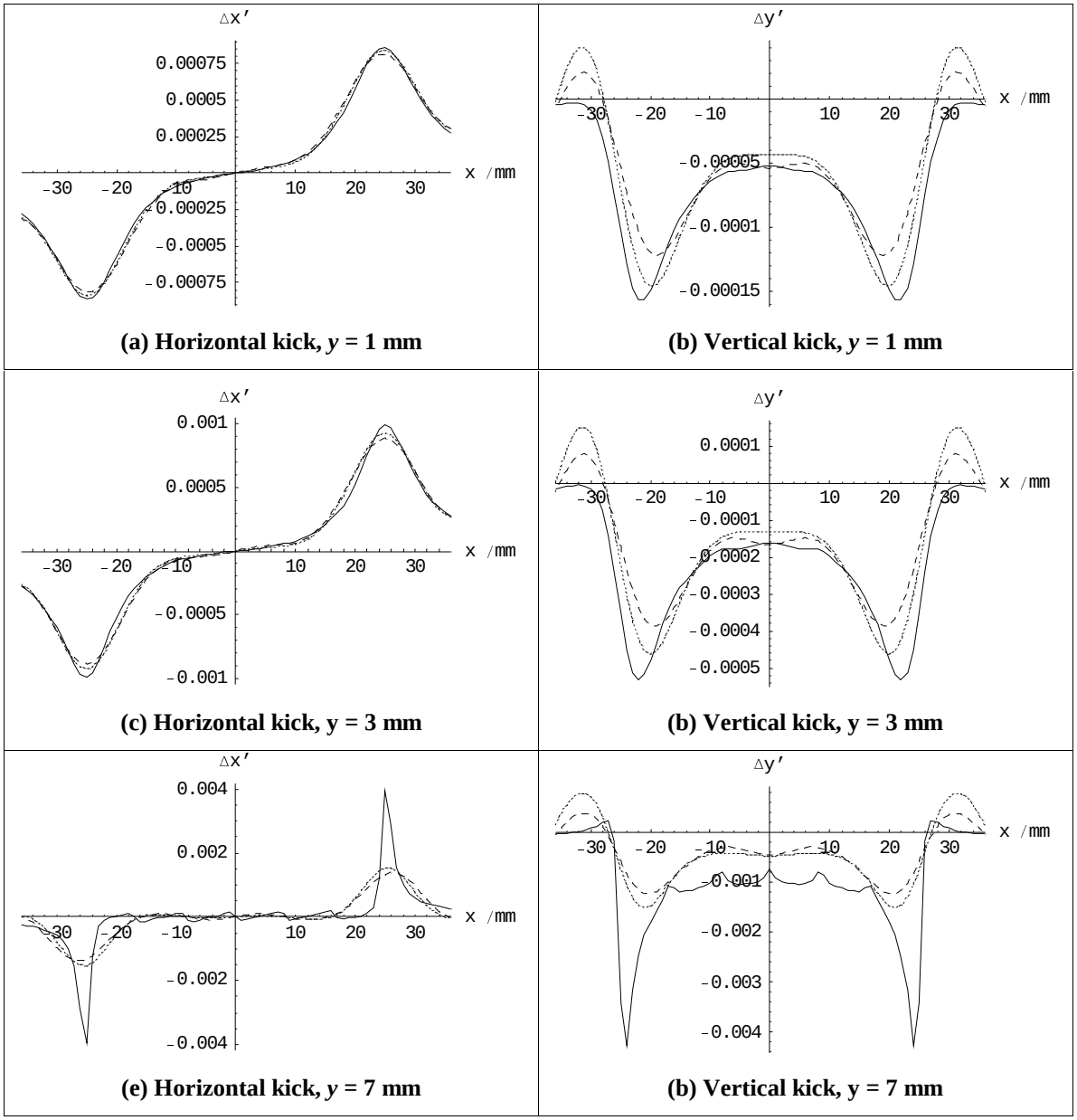

(a) Horizontal kick, y = 1 mm | **(b) Vertical kick, y = 1 mm**

(c) Horizontal kick, y = 3 mm | **(b) Vertical kick, y = 3 mm**

(e) Horizontal kick, y = 7 mm | **(b) Vertical kick, y = 7 mm**

Figure 5

Horizontal and vertical kicks in the SPEAR BL11 wiggler, as a function of x, for three different values of y. The solid line shows the RADIA model (numerical integration), while the broken lines show the full symplectic integrator (long dash) and the reduced harmonic model (short dash).

In the horizontal plane, we see the expected behaviour, with the kick increasing with the gradient of the field, and then falling off as the field strength falls off. The agreement between the three models for the horizontal kick is good, except for values of y close to the pole tip, where RADIA gives a much sharper peak than expected from either of the two analytical models. The reasons for this are not clear. For the vertical kick, the

reduced harmonic model agrees more closely with RADIA than the full symplectic integrator, which tends to give a smaller kick than the other two models.

The nonlinear wiggler fields create dynamical effects that can be measured in the storage ring; these include the tune shift with amplitude, dispersion, and dynamic aperture.

4.1 Tune Shift with Amplitude

The lowest order tune shift with amplitude can be estimated from the coefficient of the third order term in the equation of motion, i.e. by fitting a third order polynomial to the horizontal kick data shown in Figure 5(a). We note that the shape of the curve of the horizontal kick as a function of x is not well described by a polynomial, even at very high order. This emphasizes the difficulty of representing the nonlinear wiggler field by thin multipoles. By taking a small subset of the data close to the origin, however, we can obtain a reasonable fit for a cubic polynomial, although the coefficient of the third order term is sensitive to the range of data selected. We estimate the value of the coefficient to be 38 m^{-3}; tune-shift measurements on SPEAR after the insertion of BL11[3] suggest values between 43 m^{-3} and 59 m^{-3}.

4.2 Closed Orbit Shift with Momentum

An orbit displaced between x = 15 mm and x = 25 mm in the wiggler will see significant additional focusing, because of the steep gradient in B_y. This should be apparent in the dispersion at the wiggler, for example, when the orbit passes through this region as the momentum deviation is increased. There are no experimental data on this effect, because the nonlinear dynamics from BL11 have made it difficult to store beam with significant closed orbit distortion. However, we can compare the results of a dispersion simulation in MERLIN, using the reduced harmonic model, with the results of a corresponding simulation in BETA, using the numerically integrated fields in RADIA. Such a comparison is shown in Figure 6.

As expected, we see a clear effect for momentum deviations corresponding to closed orbit shifts of 15 to 25 mm: there is an apparent discontinuity in dispersion in this region, thought there are clearly stable orbits possible beyond 25 mm.

4.3 Dynamic Aperture

The adverse effects on the SPEAR performance resulting from the BL11 upgrade, have been attributed to a significant reduction in the dynamic aperture caused by nonlinear fields in the wiggler. We can again compare the results of simulations using the RADIA model with simulations using the reduced harmonic model. Figure 7 shows the dynamic aperture for the bare lattice, i.e. without BL11. After BL11 is included, both models give a significant reduction in the dynamic aperture, as shown in Figure 8 (note the change of scale from Figure 7). We note that a physical aperture, corresponding to the region within which the wiggler field is defined, must be included in the tracking.

There is good agreement between the dynamic apertures predicted by the RADIA and reduced harmonic models, both for particles with zero momentum deviation, and for particles with –0.75% momentum deviation, shown in Figure 9. We note that the kicks from the wiggler scale as E^{-2} where E is the energy of the beam. From Figure 6 we see that a momentum deviation of ±0.75% shifts the closed orbit to the region in the wiggler

where the nonlinear effects are strongest, although the different models are in agreement that there are stable closed orbits on either side of this region.

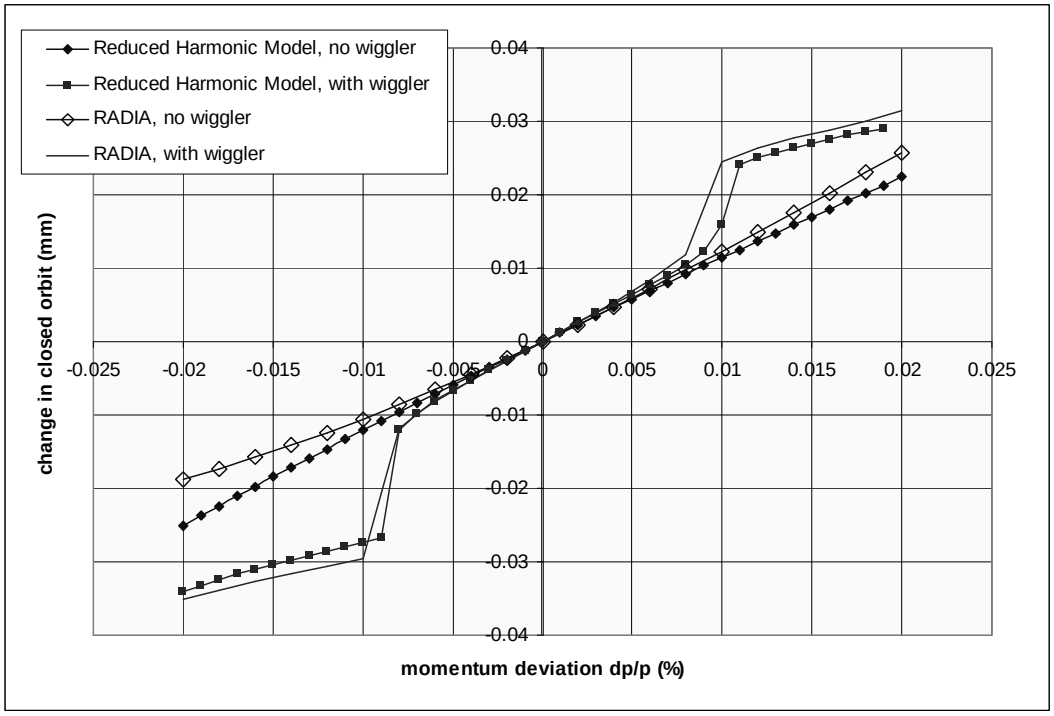

Figure 6

Comparison between closed orbit shift with momentum, simulated using the numerical integration model and the reduced harmonic model.

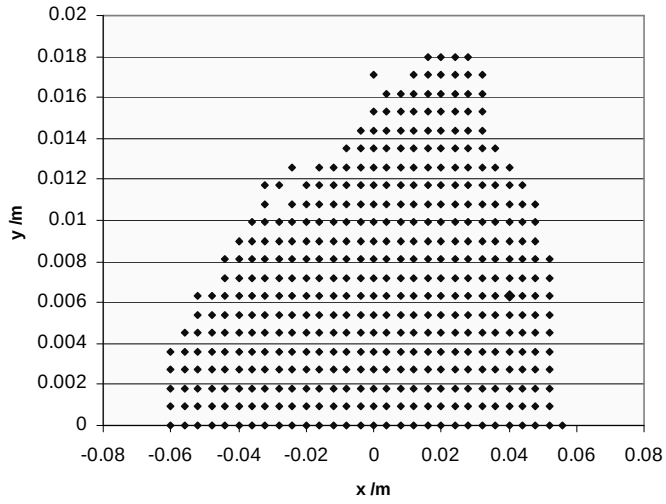

Figure 7

Dynamic aperture in the SPEAR lattice without BL11, for particles with zero momentum deviation.

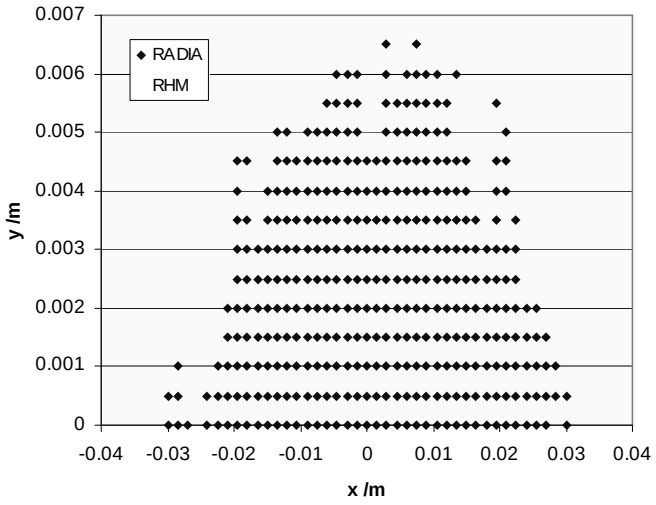

Figure 8

Dynamic aperture in the SPEAR lattice with BL11, for particles with zero momentum deviation. Points show the initial co-ordinates of stable trajectories, solid points using the RADIA model, and open points using the reduced harmonic model.

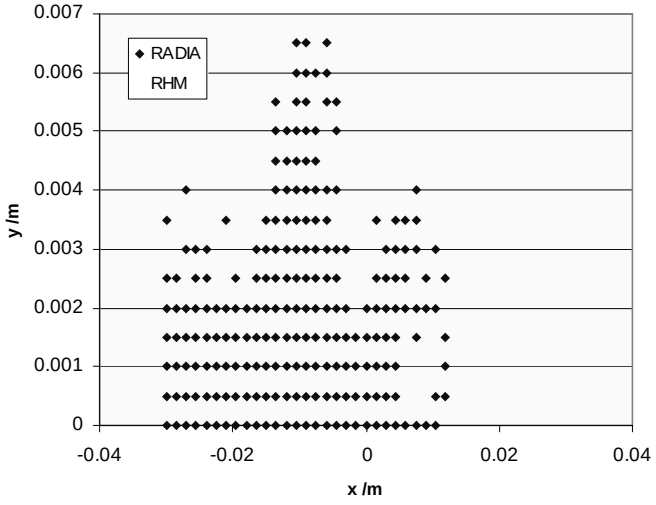

Figure 9

Dynamic aperture in the SPEAR lattice with BL11, for particles with –0.75% momentum deviation. Points show the initial co-ordinates of stable trajectories, solid points using the RADIA model, and open points using the reduced harmonic model.

4.4 Application to NLC Main Damping Rings

Tracking through over 150 wiggler periods with the field described by 79 modes slows the calculation of dynamic aperture prohibitively, even using the reduced harmonic model. We have two options:

- Reduce the number of modes used to describe the field, thus sacrificing some accuracy in the field representation. However, with the small number of modes allowed to achieve a reasonably fast tracking time, the accuracy of the fit to the field map can be expected to be poor.
- Produce a kick table by tracking one wiggler period, using a grid of starting positions. Interpolation must be used between grid points, but since a single period can be tracked very quickly, the grid may be made fine enough that the loss of accuracy will be small.

We feel that the kick table technique presents the better opportunity for fast tracking with the least loss of accuracy.

The kicks as a function of horizontal co-ordinate for three vertical positions are shown in Figure 10. We note that the peaks in the curves are beyond the range of the field data, and that the nonlinearities are significantly less severe than for the SPEAR BL11 wiggler. There is good agreement between the full symplectic integrator and the reduced harmonic model. The oscillations seen increasing in amplitude with increasing distance from the mid-plane, we believe to be artifacts from the field fitting, though some similar behaviour is seen in the SPEAR wiggler with the numerical integration of the field. This feature could warrant further investigation; for the present, we only comment that the oscillations seem less severe with the reduced harmonic model, and that we do not expect them to influence the dynamics significantly.

We find that the results of dynamics studies using the full symplectic integrator and the reduced harmonic model are, in the case of the MDR wiggler, almost identical. The results we present in the remainder of this section were obtained using the (more efficient) reduced harmonic model.

4.5 Tune Shift

The linear focusing from one period of a wiggler is given by:

$$K_1 = \frac{\overline{B_w^2}}{(B\rho)^2}$$

where $\overline{B_w^2}$ is the mean square field along the axis of the wiggler. Using the field expansion (3), we find:

$$\overline{B_w^2} = \frac{1}{2}\sum_{\substack{m,m' \\ n}} c_{mn}c_{m'n}$$

The linear model of the wiggler we used for the lattice design assumed a peak field of 2.15 T, which would give:

$$K_1 = 0.05299\ \mathrm{m}^{-2} \qquad \textbf{linear wiggler}$$

Using the coefficients of the field expansion found in section 2.2, we have:

$$K_1 = 0.05892\,\mathrm{m}^{-2}$$ **hybrid wiggler model**

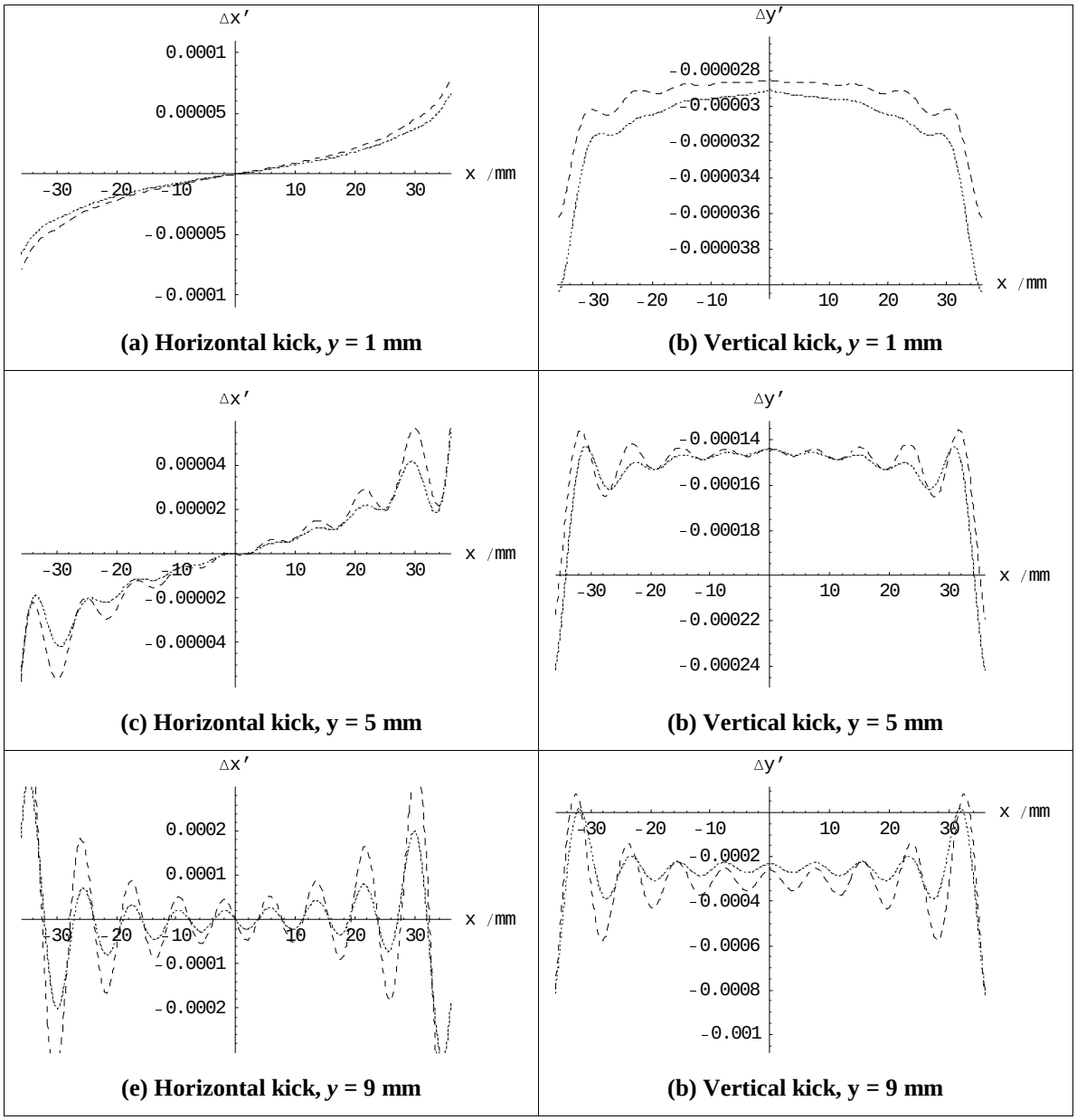

(a) Horizontal kick, *y* = 1 mm **(b) Vertical kick, *y* = 1 mm**

(c) Horizontal kick, y = 5 mm **(b) Vertical kick, y = 5 mm**

(e) Horizontal kick, *y* = 9 mm **(b) Vertical kick, y = 9 mm**

Figure 10

Horizontal and vertical kicks in the NLC MDR hybrid wiggler, as a function of x, for three different values of y. The lines show the full symplectic integrator (long dash) and the reduced harmonic model (short dash).

We can estimate the linear tune shift from:

$$\Delta\nu_y \approx \frac{\Delta K_1}{4\pi\sqrt{K_1}}\lambda_w = 2.05\times10^{-3}$$

If we model 160 periods as nonlinear components, this gives a total tune shift of approximately 0.32. We note that the hybrid wiggler does not give the full 2.15 T required, so we expect this to be a slight under-estimate. A vertical tune shift of 0.32 in one straight will significantly affect the dynamics, and will doubtless lead to a large reduction in the dynamic aperture, even before the full nonlinear effects are included. The tunes determined from tracking in MERLIN are shown in Table 1; the increase in vertical tune is 0.328, in good agreement with our estimate. The horizontal tune has reduced slightly, which is to be expected from the small horizontal defocusing that can be seen in Figure 10a.

Table 1

Linear tune shift from hybrid wiggler model

	ν_x	ν_y
Linear Wiggler	0.262	0.136
Hybrid Wiggler, $\hat{B}_w = 2.10\,\mathrm{T}$	0.239	0.464
Hybrid Wiggler, $\hat{B}_w = 1.94\,\mathrm{T}$	0.262	0.153

A rigorous analysis of the nonlinear effects of the wiggler will require retuning of the lattice to allow for the extra vertical focusing. For the present, however, we simply require an estimate of the severity of the nonlinear effects on the dynamic aperture, and achieve this by reducing the wiggler field. A reduction in the field mode coefficients by 7.5% reduces the tunes to values much closer to those appropriate for the current lattice design, without the need for retuning.

The tune shifts with amplitude with the linear model and the reduced field nonlinear model are shown in Figure 11. Horizontally, the effects of the nonlinear fields appear to be small, with deviation between the linear and nonlinear models only becoming apparent at amplitudes close to the linear model dynamic aperture. Vertically, the tune shift with amplitude appears to be reduced somewhat by the linear fields although the behaviour for amplitudes above 5 mm is somewhat unusual. This may be the effect of a resonance (a sixth order resonance appears to be strongly driven at amplitudes around 6 mm), or a consequence in the variation of the vertical kick as a function of vertical position, as shown in Figure 12. Although we might expect the vertical dynamic aperture to be more limited in the nonlinear wiggler model than in the linear case, the tune shifts with amplitude do not suggest any great cause for concern.

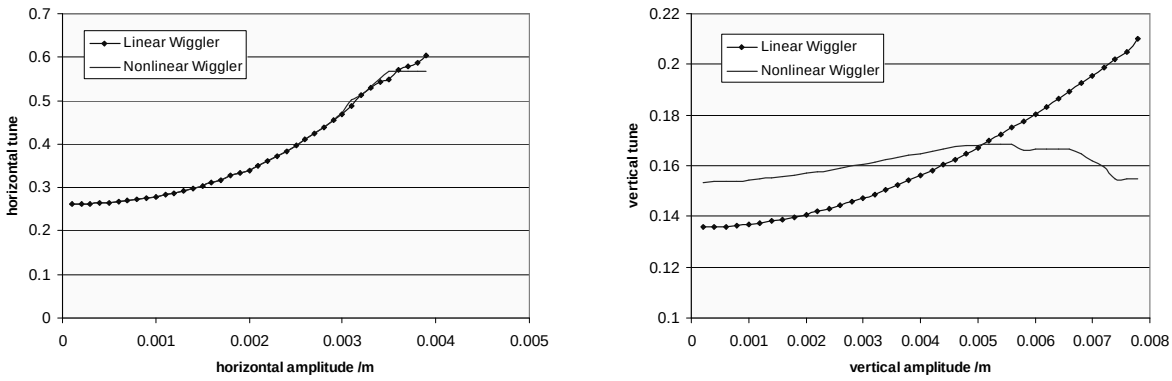

(a) **(b)**

Figure 11

Tune shift with amplitude in (a) the horizontal plane and (b) the vertical plane for the linear and nonlinear wiggler models.

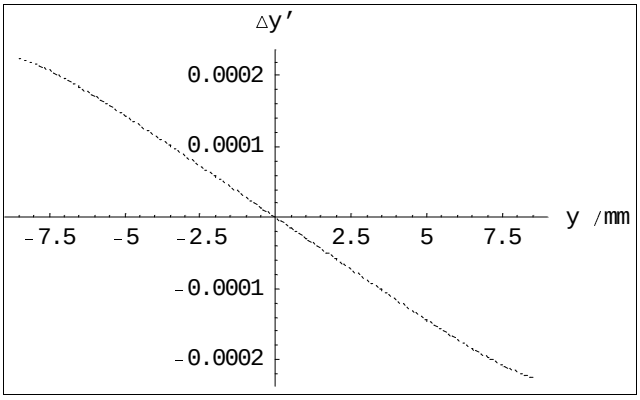

Figure 12

Vertical kick from one wiggler period as a function of vertical position.

4.6 Dynamic Aperture

The problem we face with tracking the nonlinear wiggler is that the momentum kicks are only defined over a finite region of space. Conventionally, for dynamic aperture studies, one assumes that all multipole fields extend to infinity, and physical apertures are only included in tracking when calculating the full acceptance. For studies of the nonlinear wiggler, we are forced to collimate at horizontal and vertical positions that correspond to the defined limits within which the field is known and has been fitted. In the case of the hybrid wiggler, the limits are ±40 mm horizontally, and ±9 mm vertically. We note that the physical aperture will actually be the beam pipe of 8 mm radius in the wiggler. Attempts have been made in recent revisions of the lattice design, to reduce the size of the beta functions in the wiggler; lattice functions in the wiggler straight are shown in Figure 13. We feel it will be difficult to reduce the beta functions below peak values of 10 m and 12 m, for the horizontal and vertical planes respectively.

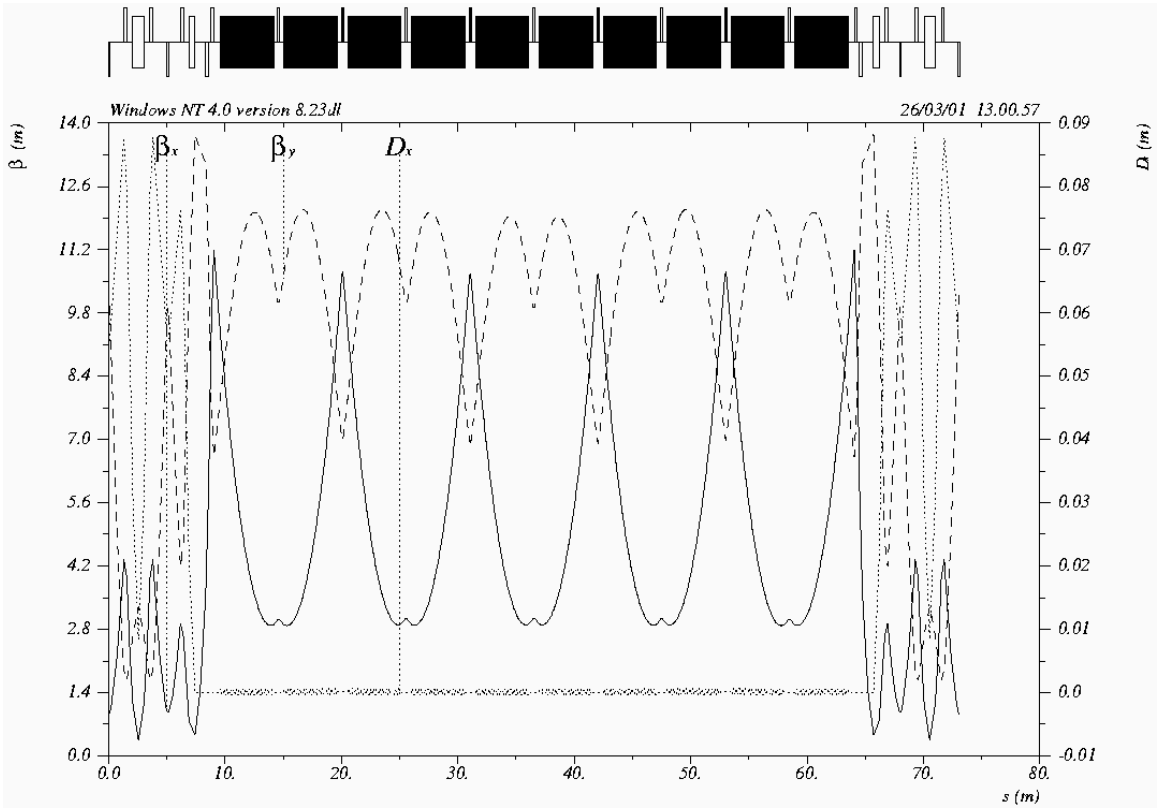

Figure 13

Lattice functions in the wiggler straight of the MDR

The dynamic aperture of the lattice with the wiggler modeled as a linear element (sequence of dipoles) is shown in Figure 14(a). We note that with no collimation, the dynamic aperture is significantly larger than fifteen times the injected beam size. With collimation applied in the wiggler, corresponding to the limits of the nonlinear field model, there is a significant reduction in the vertical aperture. The dynamic aperture with the reduced harmonic model of the nonlinear wiggler, and with collimation at ±40 mm horizontally, ±9 mm vertically, is shown in Figure 15(a). Although it appears that the dynamic aperture is the limiting effect, nonlinear terms in the equation of motion can drive betatron oscillations with larger amplitude than expected, so stable orbits that might be expected to stay within the physical aperture may in fact venture outside. Comparison with Figure 14(b), where the aperture is limited by collimation, suggests that the collimation is again the limiting factor in the nonlinear model.

We can test the effect of the expected actual physical aperture of 8 mm radius beam pipe in the wiggler. The results are shown in Figure 15(b). In this case, the physical aperture is clearly the limiting quantity, and restricts the on-energy acceptance to (roughly) ten times the injected beam size.

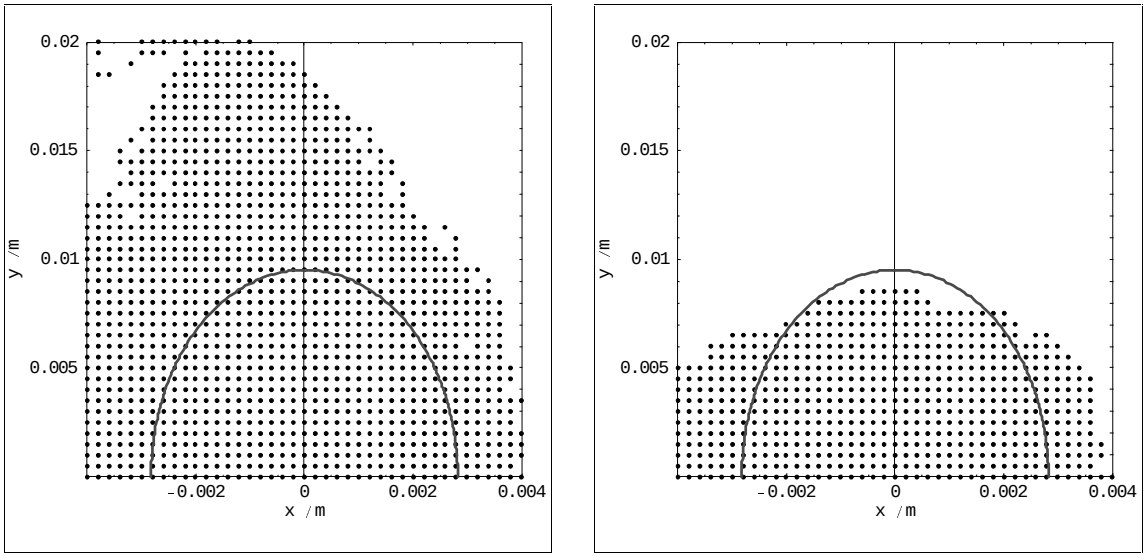

(a) **(b)**

Figure 14

Dynamic aperture of the NLC main damping rings with the wiggler modeled as a linear element. The half ellipse shows fifteen times the injected beam size. (a) No collimation; (b) beam collimated in the wiggler at $x = \pm 0.04$ m and $y = \pm 0.009$ m.

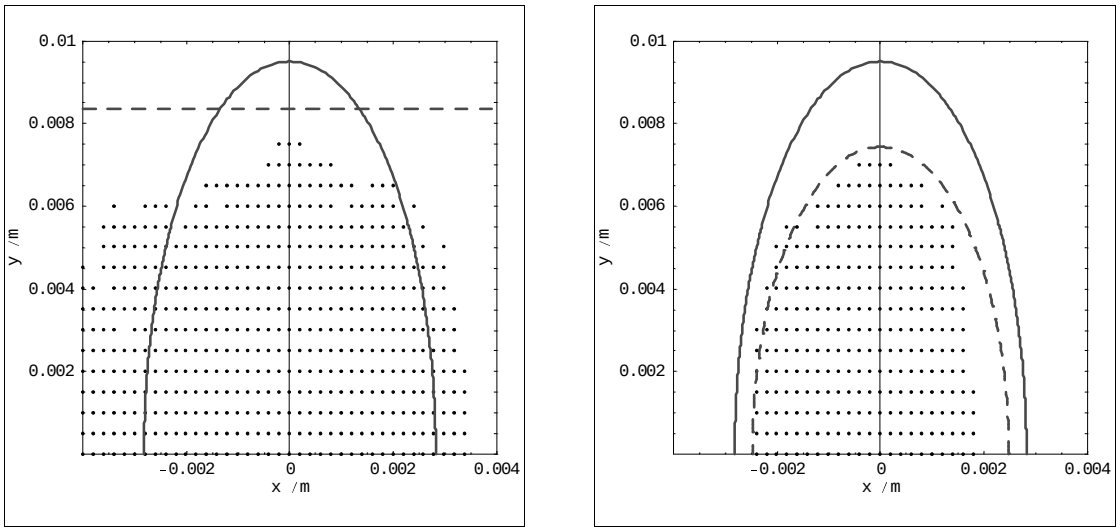

(a) **(b)**

Figure 15

Dynamic aperture with the nonlinear wiggler model. The solid ellipse shows fifteen times the injected beam size, and the horizontal broken line shows the physical aperture scaled to the beta functions at the observation point (the center of the defocusing quadrupole in an arc cell). In (a) the beam is collimated in the wiggler at ±40 mm horizontally, ±9 mm vertically, and in (b) the collimation is at the beam pipe radius of 8 mm.

5 Conclusions

We have found it possible in the case of the SPEAR BL11 wiggler and the NLC MDR wiggler, to construct a mode expansion for the field that reproduces the modeled field with good accuracy, with rms deviation of the order 0.1% of the peak field, in the best case. The mode expansion allows us to construct a symplectic integrator for mapping through periods of the wiggler. Comparison with numerical integration techniques supports the validity of our models.

The SPEAR BL11 wiggler shows strong nonlinear effects, resulting from a rapid roll-off of the vertical field, within the dynamic aperture of the bare lattice. The hybrid wiggler proposed for the MDR shows a much smaller roll-off in the field, though the nonlinear effects are still significant, as a result of the length of the wiggler (160 periods modeled as nonlinear elements). To avoid the need to retune the lattice to correct for the linear tune shift, we tracked the wiggler with a reduced field, 1.98 T as opposed to 2.15 T peak field. We find that there is significant reduction in the aperture, though it appears that the dominant effect is the physical collimation; certainly in the case where the 8 mm radius beam pipe is included as a hard aperture, the acceptance is limited by collimation.

Acknowledgements

I should like to thank Ying Wu of LBNL for useful discussions on the material presented in this note, and particularly for explaining to me his model of the wiggler, which I refer to as the "full symplectic integrator". I should also like to thank James Safranek and Cecile Limborg of SSRL, for providing data on the SPEAR BL11 wiggler, and for their helpful comments and suggestions. Thanks also to Steve Marks of LBNL for providing data on the NLC MDR hybrid wiggler design.

References

[1] The NLC Design Group, "*Zeroth-Order Design Report for the Next Linear Collider*" (Chapter 4), LBNL-PUB-5424, SLAC Report 474, 1996.

[2] A. Wolski, "*Lattice Description for NLC Main Damping Rings at 120 Hz*", CBP Technical Note 227, LCC-0061, April 2001.

[3] J. Safranek, C. Limborg, A. Terebilo, K.I. Blomqvist, P.Elleaume, Y. Nosochkov, "*Nonlinear Dynamics in SPEAR Wigglers*", Proc. EPAC 2000.

[4] P. Elleaume, O. Chubar, J. Chavanne, "*Computing 3D Magnetic Fields from Insertion Devices*", Proc. PAC 1997.

[5] http://www.desy.de/~njwalker/MerlinII/index.htm